6×6 effective mass Hamiltonian for heterostructures grown on (11*N*)-oriented substrates

Woon-Ho Seo and John F. Donegan
Semiconductor Photonics Group, Department of Physics, Trinity College Dublin, Dublin2, Ireland
(Received 17 January 2003; published 27 August 2003)

The 6×6 effective mass Hamiltonian for semiconductor heterostructures grown on (11*N*)-oriented substrates is derived and is compared with the 4×4 model. The hole subbands of InGaAs/InP single quantum wells grown on (11*N*)-oriented substrates with $N=\infty$ (that is, (001)], 0, 1 are calculated using the effective mass Hamiltonian as an example. The spin-orbit coupling affects the light-hole subband at $k_{||}=0$, but it affects all subbands at finite $k_{||}$ for all substrate orientations. In the 4×4 model (without spin-orbit coupling), the coupling between the heavy hole and the light hole is overestimated. At a critical uniaxial stress, the position of the first heavy hole and the first light hole as the highest energy level cross over. The separation between the first heavy hole and the first light hole is overestimated at the uniaxial stress below the critical value and is underestimated above the critical stress in the 4×4 model. The spin-orbit coupling greatly affects the valence band structures of the semiconductor heterostructures resulting in the modifications of the optical transitions anisotropy for structures grown on (11*N*)-oriented substrates.

DOI: 10.1103/PhysRevB.68.075318 PACS number(s): 73.21.Fg

I. INTRODUCTION

Recently, many semiconductor heterostructures have been successfully grown on high-index substrates.[1–6] The growth of GaAs/(Al,Ga)As quantum wells (QW's) on non-(001)-oriented substrates has attracted much interest for its potential in the fabrication of semiconductor nanostructures having better crystallographic morphology. The self-organizing growth mechanisms on planar and patterned high-index semiconductor surfaces leading to high quality quantum wires (QWR's) and quantum dots (QD's) have been developed in GaAs materials.[4,5] Also, high quality QD's with uniform size distributions on high-index InP substrates have been fabricated.[6] According to the substrate orientation, the anisotropy in the interband optical transitions is changed reflecting the inherent anisotropy of the materials and the quantum confinement of electronic systems. Moreover, the anisotropy reveals the crystal direction which generates the most intense optical transitions. This information is very important for optical device applications. For the interpretation of the physical phenomena in these heterostructures grown on high-index substrates, a detailed understanding of the valence band mixing is needed. Effective mass theory is widely used to calculate the energy band structures in semiconductor systems. The 4×4 and 6×6 Luttinger-Kohn models[7,8] and the 6×6 and 8×8 Kane models[9–12] have been used for the heterostructures grown on (001)-oriented substrate. Xia has proposed an effective mass theory for superlattices grown on (11*N*)-oriented substrates based on Luttinger's theory with a 4×4 matrix including the coupling between the heavy and light holes.[13] Optical transitions involving the spin-orbit split-off bands in GaAs/AlGaAs (Ref. 14) and strained ZnSe/ZnS (Ref. 15) superlattices have been observed. The strain effect introduces additional coupling between heavy-hole (HH) and light-hole (LH) bands, and spin-orbit split-off (SO) bands.[16] Therefore the inclusion of SO bands in valence band mixing is crucial for the explanation of the physical properties of semiconductor heterostructures. According to Bahder, the strain effect introduces a wave vector dependent conduction-valence bands mixing.[10] In this paper, we will mainly focus on the mixing in valence band, therefore we choose to neglect the coupling between conduction band and valence band.

The purpose of this paper is to illustrate the coupling between the HH, LH, and the SO bands with the strain in the heterostructures grown on (11*N*)-oriented substrates. The Kane model with spin-orbit coupling is derived in the basis of *p*-like states $|X\rangle\uparrow,|Y\rangle\uparrow,|Z\rangle\uparrow,|X\rangle\downarrow,|Y\rangle\downarrow,|Z\rangle\downarrow$ and is changed into the 6×6 Luttinger-Kohn model in angular momentum basis $|jm_j\rangle$ with $j=\frac{3}{2},\frac{1}{2}$ by the unitary transformation for the structures grown on (110)-, (111)-, (112)-, (113)-, and (11∞)-oriented substrates. The hole subband structures, the effect of the uniaxial stress along the growth direction are studied and compared for each substrate orientation with and without spin-orbit coupling.

II. THEORY

A. Effective mass theory

The three axes of the coordinate system used in this paper are defined as follows: the three axis is along the growth direction, the two axis is in the $[\bar{1}10]$ direction, and the one and three axes in the $(\bar{1}10)$ plane. θ is the angle between the three axis and the *x*-*y* plane where *x*,*y*,*z* axes are the three directions of the primitive vectors of a simple cubic Bravais lattice; as θ varies from 0 to $\pi/2$, the growth plane perpendicular to the three axis changes from (110) in succession to (111),(112),(113),(11∞), i.e., (001). Making the coordinate transform

$$k_x=\frac{s}{\sqrt{2}}k_1-\frac{1}{\sqrt{2}}k_2+\frac{c}{\sqrt{2}}k_3,$$

$$k_y=\frac{s}{\sqrt{2}}k_1+\frac{1}{\sqrt{2}}k_2+\frac{c}{\sqrt{2}}k_3,$$

$$k_z=-ck_1+sk_3, \tag{1}$$

TABLE I. Values of a,b,d,e,f,g for matrices $A,B,C,\ldots,F',G'$.

	a	b	d	e	f	g
A	$\frac{s^2}{2}+\frac{3s^2c^2}{2}$	0	$-\frac{s^3c}{2}+sc^3$	$\frac{1}{2}s^2+c^2$	0	$\frac{s^4}{2}+\frac{s^2}{2}+c^4$
B	$\frac{1}{2}+\frac{c^2}{2}$	0	$-\frac{sc}{2}$	$\frac{1}{2}$	0	$\frac{1}{2}+\frac{s^2}{2}$
C	$\frac{c^2}{2}+\frac{c^4}{2}+s^4$	0	$-\frac{s^3c}{2}+s^3c$	$\frac{c^2}{2}+s^2$	0	$\frac{3s^2c^2}{2}+\frac{c^2}{2}$
D	0	$-s^2$	0	0	$-sc$	0
F	0	$-sc$	0	0	$-c^2$	0
G	$sc+sc^3-2s^3c$	0	$-3s^2c^2$	$-sc$	0	$s^3c+sc-2sc^3$
A'	$-\frac{s^2}{4}-\frac{3s^2c^2}{4}$	0	$\frac{s^3c}{4}-\frac{sc^3}{2}$	$\frac{s^2}{4}$	0	$\frac{s^4}{4}-\frac{s^2}{4}+s^2c^2$
B'	$\frac{1}{4}-\frac{c^2}{4}$	0	$\frac{sc}{4}$	$-\frac{1}{4}$	0	$\frac{1}{4}-\frac{s^2}{4}$
C'	$-\frac{c^2}{4}+\frac{c^4}{4}+s^2c^2$	0	$\frac{sc^3}{4}-\frac{s^3c}{2}$	$\frac{c^2}{4}$	0	$-\frac{3s^2c^2}{4}-\frac{c^2}{4}$
D'	0	$-\frac{c^2}{2}$	0	0	$\frac{sc}{2}$	0
F'	0	$\frac{sc}{2}$	0	0	$-\frac{s^2}{2}$	0
G'	$-\frac{sc}{2}-\frac{sc^3}{2}+s^3c$	0	$\frac{s^2c^2}{2}-\frac{s^4}{2}-\frac{c^4}{2}$	$\frac{sc}{2}$	0	$sc^3-\frac{s^3c}{2}-\frac{sc}{2}$

$$J_x=\frac{s}{\sqrt{2}}J_1-\frac{1}{\sqrt{2}}J_2+\frac{c}{\sqrt{2}}J_3,$$

$$J_y=\frac{s}{\sqrt{2}}J_1+\frac{1}{\sqrt{2}}J_2+\frac{c}{\sqrt{2}}J_3,$$

$$J_z=-cJ_1+sJ_3, \tag{2}$$

where s and c represent $\sin\theta$ and $\cos\theta$, respectively. And the matrices J_i in the bases X,Y,Z are

$$J_1=\begin{Vmatrix} 0 & 0 & 0 \\ 0 & 0 & -i \\ 0 & i & 0 \end{Vmatrix}, \quad J_2=\begin{Vmatrix} 0 & 0 & i \\ 0 & 0 & 0 \\ -i & 0 & 0 \end{Vmatrix},$$

$$J_3=\begin{Vmatrix} 0 & -i & 0 \\ i & 0 & 0 \\ 0 & 0 & 0 \end{Vmatrix}. \tag{3}$$

Inserting Eqs. (1) and (2) into the 3×3 Kane Hamiltonian in X,Y,Z bases for hole energy states[17]

$$H_I=Lk^2\mathbf{I}-(L-M)(k_x^2J_x^2+k_y^2J_y^2+k_z^2J_z^2)-2N(k_xk_y[J_xJ_y]+k_yk_z[J_yJ_z]+k_xk_z[J_xJ_z]), \tag{4}$$

we obtain the 3×3 effective mass Hamiltonian in the (1,2,3) coordinate system

$$H_I=Lk^2\mathbf{I}-(L-M)(Ak_1^2+Bk_2^2+Ck_3^2+Dk_1k_2+Fk_2k_3+Gk_1k_3)-2N(A'k_1^2+B'k_2^2+C'k_3^2+D'k_1k_2+F'k_2k_3+G'k_1k_3), \tag{5}$$

where $A,B,C,\ldots,F',G'$ are 3×3 matrices which have the following form:

$$X=\begin{pmatrix} a & b & d \\ b & e & f \\ d & f & g \end{pmatrix}. \tag{6}$$

Values of a,b,d,e,f,g which are functions of s and c for each matrix are presented in Table I. For constructing the 6×6 Kane Hamiltonian, the set of spin-dependent basis functions $|m\sigma\rangle$ with $m=X,Y,Z$ for Γ_{15} valence band states, and $\sigma=\uparrow,\downarrow$ for spin-up and spin-down spinors $|X\uparrow\rangle,|Y\uparrow\rangle,|Z\uparrow\rangle,|X\downarrow\rangle,|Y\downarrow\rangle,|Z\downarrow\rangle$ are introduced. The total Hamiltonian is composed of the $\mathbf{k}\cdot\mathbf{p}$ part $H_{k\cdot p}$, and the spin-orbit interaction part H_{SO}

$$H_{k\cdot p}=\begin{pmatrix} H_I & 0 \\ 0 & H_I \end{pmatrix} \tag{7}$$

and the spin-orbit interaction matrix in these bases is given by the expression

$$H_{\mathrm{SO}}=\frac{\Delta}{3}\begin{pmatrix} -i & 0 & 0 & 0 & 0 & 1 \\ i & 0 & 0 & 0 & 0 & -i \\ 0 & 0 & 0 & -1 & i & 0 \\ 0 & 0 & -1 & 0 & i & 0 \\ 0 & 0 & -i & -i & 0 & 0 \\ 1 & i & 0 & 0 & 0 & 0 \end{pmatrix}, \tag{8}$$

where Δ is the spin-orbit split-off energy. This is diagonal in the angular momentum basis $|jm_j\rangle$ with $j=\frac{3}{2},\frac{1}{2}$ for the four Γ_8 heavy and light hole states and the two Γ_7 spin-orbit split-off states, taking the values $\Delta/3,-2\Delta/3$, respectively. The new basis functions are generated by means of a unitary transformation

$$|jm_j\rangle=\sum_{m\sigma} U_{m\sigma,jm_j}|m\sigma\rangle, \tag{9}$$

where

$$U_{m\sigma,jm_j}=\begin{pmatrix} -\frac{1}{\sqrt{2}} & 0 & \frac{1}{\sqrt{6}} & 0 & 0 & \frac{1}{\sqrt{3}} \\ -\frac{i}{\sqrt{2}} & 0 & -\frac{i}{\sqrt{6}} & 0 & 0 & -\frac{i}{\sqrt{3}} \\ 0 & \sqrt{\frac{2}{3}} & 0 & 0 & \frac{1}{\sqrt{3}} & 0 \\ 0 & -\frac{1}{\sqrt{6}} & 0 & \frac{1}{\sqrt{2}} & \frac{1}{\sqrt{3}} & 0 \\ 0 & -\frac{i}{\sqrt{6}} & 0 & -\frac{i}{\sqrt{2}} & \frac{i}{\sqrt{3}} & 0 \\ 0 & 0 & \sqrt{\frac{2}{3}} & 0 & 0 & -\frac{1}{\sqrt{3}} \end{pmatrix}, \tag{10}$$

$$\left|\frac{3}{2},\frac{3}{2}\right\rangle=-\frac{1}{\sqrt{2}}|(X+iY)\uparrow\rangle,$$

$$\left|\frac{3}{2},\frac{1}{2}\right\rangle=-\frac{1}{\sqrt{6}}|(X+iY)\downarrow\rangle+\sqrt{\frac{2}{3}}|Z\uparrow\rangle,$$

$$\left|\frac{3}{2},-\frac{1}{2}\right\rangle=\frac{1}{\sqrt{6}}|(X-iY)\uparrow\rangle+\sqrt{\frac{2}{3}}|Z\downarrow\rangle,$$

$$\left|\frac{3}{2},-\frac{3}{2}\right\rangle=\frac{1}{\sqrt{2}}|(X-iY)\downarrow\rangle,$$

$$\left|\frac{1}{2},\frac{1}{2}\right\rangle=\frac{1}{\sqrt{3}}|(X+iY)\downarrow\rangle+\frac{1}{\sqrt{3}}|Z\uparrow\rangle,$$

$$\left|\frac{1}{2},-\frac{1}{2}\right\rangle=\frac{1}{\sqrt{3}}|(X-iY)\uparrow\rangle-\frac{1}{\sqrt{3}}|Z\downarrow\rangle. \tag{11}$$

Luttinger parameters are given in terms of Kane parameters

$$\gamma_1=-\frac{2}{3}\frac{m_0}{\hbar^2}(L+2M),$$

$$\gamma_2=-\frac{1}{3}\frac{m_0}{\hbar^2}(L-M),$$

$$\gamma_3=-\frac{1}{3}\frac{m_0}{\hbar^2}N. \tag{12}$$

From Eq. (5), Table I, and unitary transformation, the 6×6 effective-mass Hamiltonian can be obtained for heterostructures grown on (11N)-oriented substrates, for $N=0,c=1,s=0$; $N=1,c=\sqrt{2/3},s=1/\sqrt{3}$; $N=2,c=1/\sqrt{3},s=\sqrt{2/3}$; $N=3,c=\sqrt{2/11},s=3/\sqrt{11}$; $N=\infty,c=0,s=1$; etc. The matrix has the following form:

TABLE II. Values of $P,Q,R,$ and S for the matrix in Eq. (13) for $(11N)$-oriented substrates.

$N=0$	$P=-\gamma_1 k^2$
	$Q=-\frac{\gamma_2}{2}(2k_1^2-k_2^2-k_3^2)-\frac{3}{2}\gamma_3(k_2^2-k_3^2)$
	$S=2\sqrt{3}(\gamma_3 k_1 k_3 - i\gamma_2 k_2 k_3)$
	$R=\frac{\sqrt{3}}{2}\{\gamma_2(2k_1^2-k_2^2-k_3^2)-\gamma_3[(k_2^2-k_3^2)+i4k_1k_2]\}$
$N=1$	$P=-\gamma_1 k^2$
	$Q=-\gamma_3(k_1^2+k_2^2-2k_3^2)$
	$S=-\frac{\sqrt{6}}{3}(\gamma_2-\gamma_3)(k_1+ik_2)^2+\frac{2\sqrt{3}}{3}(2\gamma_2+\gamma_3)(k_1-ik_2)k_3$
	$R=\frac{\sqrt{3}}{3}(\gamma_2+2\gamma_3)(k_1-ik_2)^2-\frac{2\sqrt{6}}{3}(\gamma_2-\gamma_3)(k_1+ik_2)k_3$
$N=2$	$P=-\gamma_1 k^2$
	$Q=-\frac{\gamma_2}{2}(k_2^2-k_3^2+2\sqrt{2}k_1k_3)-\frac{\gamma_3}{2}(2k_1^2+k_2^2-3k_3^2-2\sqrt{2}k_1k_3)$
	$S=\frac{\sqrt{6}}{3}\gamma_2[(k_2^2-k_3^2+2\sqrt{2}k_1k_3)-i(2k_1k_2+\sqrt{2}k_2k_3)]$
	$-\frac{\sqrt{6}}{3}\gamma_3[(k_2^2-k_3^2-2\sqrt{2}k_1k_3)-i(2k_1k_2-\sqrt{2}k_2k_3)]$
	$R=-\frac{\sqrt{3}}{6}\gamma_2[(k_2^2-k_3^2+2\sqrt{2}k_1k_3)+i(8k_1k_2+4\sqrt{2}k_2k_3)]$
	$+\frac{\sqrt{3}}{6}\gamma_3[(6k_1^2-5k_2^2-k_3^2+2\sqrt{2}k_1k_3)-i(4k_1k_2-4\sqrt{2}k_2k_3)]$
$N=3$	$P=-\gamma_1 k^2$
	$Q=-\frac{8}{121}\gamma_2(5k_1^2+11k_2^2-16k_3^2+18\sqrt{2}k_1k_3)-\frac{3}{121}\gamma_3(27k_1^2+11k_2^2-38k_3^2-48\sqrt{2}k_1k_3)$
	$S=-\frac{\sqrt{6}}{121}\gamma_2[(15k_1^2+33k_2^2-48k_3^2+54\sqrt{2}k_1k_3)-i(66k_1k_2+22\sqrt{2}k_2k_3)]$
	$-\frac{\sqrt{6}}{121}\gamma_3[(15k_1^2+33k_2^2-48k_3^2-67\sqrt{2}k_1k_3)-i(66k_1k_2-33\sqrt{2}k_2k_3)]$
	$R=-\frac{\sqrt{3}}{121}\gamma_2[(5k_1^2+11k_2^2-16k_3^2+18\sqrt{2}k_1k_3)+i(198k_1k_2+66\sqrt{2}k_2k_3)]$
	$+\frac{2\sqrt{3}}{121}\gamma_3[(63k_1^2-55k_2^2-8k_3^2+9\sqrt{2}k_1k_3)-i(22k_1k_2-33\sqrt{2}k_2k_3)]$
$N=\infty$	$P=-\gamma_1 k^2$
	$Q=-\gamma_2(k_1^2+k_2^2-2k_3^2)$
	$S=2\sqrt{3}\gamma_3(k_1-ik_2)k_3$
	$R=\sqrt{3}[\gamma_3(k_1^2-k_2^2)-i2\gamma_2 k_1k_2]$

$$H=\frac{\hbar^2}{2m_0}\begin{pmatrix} P+Q & S & R & 0 & \frac{1}{\sqrt{2}}S & \sqrt{2}R \\ S^\dagger & P-Q & 0 & R & -\sqrt{2}Q & -\sqrt{\frac{3}{2}}S \\ R^\dagger & 0 & P-Q & -S & -\sqrt{\frac{3}{2}}S^\dagger & \sqrt{2}Q \\ 0 & R^\dagger & -S^\dagger & P+Q & -\sqrt{2}R^\dagger & \frac{1}{\sqrt{2}}S^\dagger \\ \frac{1}{\sqrt{2}}S^\dagger & -\sqrt{2}Q & -\sqrt{\frac{3}{2}}S & -\sqrt{2}R & P-\Delta & 0 \\ \sqrt{2}R^\dagger & -\sqrt{\frac{3}{2}}S^\dagger & \sqrt{2}Q & \frac{1}{\sqrt{2}}S & 0 & P-\Delta \end{pmatrix}. \quad (13)$$

The values of P,Q,R,S in Eq. (13) for $(11N)$-oriented substrates where $N=0,1,2,3,$ and ∞ are presented in Table II.

B. Uniaxial stress effects

In this section the effects of external uniaxial stress along the growth direction are discussed. In X,Y,Z bases the strain Hamiltonian caused by a homogeneous strain is given by[17]

$$H_I(\varepsilon)=\begin{vmatrix} l\varepsilon_{xx}+m(\varepsilon_{yy}+\varepsilon_{zz}) & n\varepsilon_{xy} & n\varepsilon_{xz} \\ n\varepsilon_{xy} & l\varepsilon_{yy}+m(\varepsilon_{xx}+\varepsilon_{zz}) & n\varepsilon_{yz} \\ n\varepsilon_{xy} & n\varepsilon_{xz} & l\varepsilon_{xx}+m(\varepsilon_{yy}+\varepsilon_{zz}) \end{vmatrix} \tag{14}$$

where $l=D_{xx}^{XX}, m=D_{yy}^{XX}, n=D_{xy}^{XY}$ are the deformation potentials. This can be expressed as a form similar to a 3×3 Kane Hamiltonian:

$$H_I(\varepsilon)=l\varepsilon I-(l-m)(\varepsilon_{xx}J_x^2+\varepsilon_{yy}J_y^2+\varepsilon_{zz}J_z^2) -2n(\varepsilon_{xy}[J_xJ_y]+\varepsilon_{xz}[J_xJ_z]+\varepsilon_{yz}[J_yJ_z]). \tag{15}$$

In the case of the uniaxial stress T along the growth direction (that is, three axis), the stress tensor components

$$T_{\alpha\beta}=\tau_\alpha\tau_\beta T, \quad \alpha,\beta=x,y,z, \tag{16}$$

$$\tau_x=\tau_y=\frac{c}{\sqrt{2}}, \tau_z=s, \tag{17}$$

and the strain tensor components

$$\varepsilon_{xx}=[(S_{11}-S_{12})\tau_x^2+S_{12}]T =\left[\left(\frac{1}{C_{11}-C_{12}}\tau_x^2\right)\tau_x^2 -\frac{C_{12}}{(C_{11}+2C_{12})(C_{11}-C_{12})}\right]T, \quad \text{c.p.},$$

$$\varepsilon_{xy}=\frac{1}{2}S_{44}\tau_x\tau_yT=\frac{1}{2}\frac{1}{C_{44}}\tau_x\tau_yT, \quad \text{c.p.}, \tag{18}$$

where S_{11},S_{12},S_{44} are the cubic elastic compliance constants, C_{11},C_{12},C_{44} are the elastic stiffness constants, and c.p. refers to the terms obtained by the cyclic permutation of indices. From Eq. (18) it can be obtained that

$$\varepsilon_{xx}+\varepsilon_{yy}+\varepsilon_{zz}=(S_{11}+2S_{12})T=\left(\frac{1}{C_{11}+2C_{12}}\right)T \tag{19}$$

is independent of orientation, i.e., this term represents a constant energy shift. Using Eq. (18) the Hamiltonian in Eq. (15) can be rewritten as

$$H_I(\varepsilon)=lC_aI-(l-m)\{(C_b\tau_x^2-C_d)J_x^2+(C_b\tau_y^2-C_d)J_y^2 +(C_b\tau_z^2-C_d)J_z^2\}-2nC_f\{\tau_x\tau_y[J_xJ_y]+\tau_x\tau_z[J_xJ_z] +\tau_y\tau_z[J_yJ_z]\}, \tag{20}$$

where

$$C_a=\frac{T}{C_{11}+2C_{12}}, \quad C_d=\frac{C_{12}T}{(C_{11}+2C_{12})(C_{11}-C_{12})},$$

$$C_b=\frac{T}{C_{11}-C_{12}}, \quad C_f=\frac{T}{2C_{44}}, \tag{21}$$

and I is 3×3 identity matrix, respectively. The Pikus-Bir deformation constants a_v, b, and d are related to the deformation potentials l,m,n in Eq. (14) by

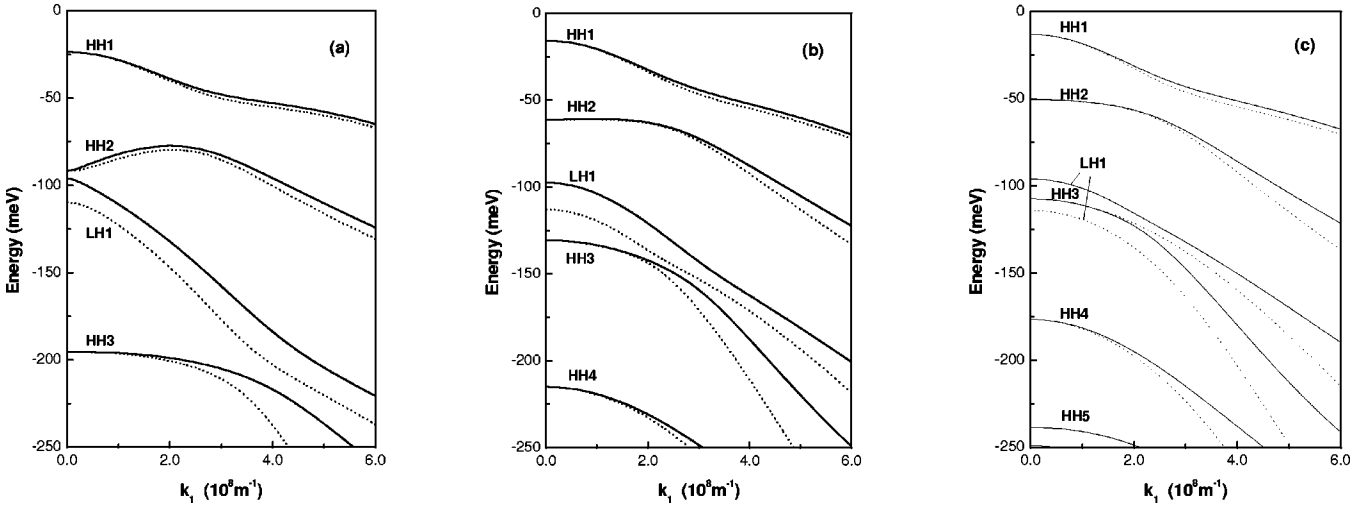

FIG. 1. Hole subbands for the $In_{0.53}Ga_{0.47}As/InP$ quantum wells grown on $(11N)$-oriented substrates with (a) $N=\infty$, (b) $N=0$, (c) $N=1$.

$$a_v=\frac{l+2m}{3},\quad b=\frac{l-m}{3},\quad d=\frac{n}{\sqrt{3}}. \tag{22}$$

With the same procedures, the 6×6 strain Hamiltonian in the angular momentum basis can be written as

$$H(\varepsilon)=\begin{pmatrix} P_\varepsilon+Q_\varepsilon & S_\varepsilon & R_\varepsilon & 0 & \frac{1}{\sqrt{2}}S_\varepsilon & \sqrt{2}R_\varepsilon \\ S_\varepsilon & P_\varepsilon-Q_\varepsilon & 0 & R_\varepsilon & -\sqrt{2}Q_\varepsilon & -\sqrt{\frac{3}{2}}S_\varepsilon \\ R_\varepsilon & 0 & P_\varepsilon-Q_\varepsilon & -S_\varepsilon & -\sqrt{\frac{3}{2}}S_\varepsilon & \sqrt{2}Q_\varepsilon \\ 0 & R_\varepsilon & -S_\varepsilon & P_\varepsilon+Q_\varepsilon & -\sqrt{2}R_\varepsilon & \frac{1}{\sqrt{2}}S_\varepsilon \\ \frac{1}{\sqrt{2}}S_\varepsilon & -\sqrt{2}Q_\varepsilon & -\sqrt{\frac{3}{2}}S_\varepsilon & -\sqrt{2}R_\varepsilon & P_\varepsilon & 0 \\ \sqrt{2}R_\varepsilon & -\sqrt{\frac{3}{2}}S_\varepsilon & \sqrt{2}Q_\varepsilon & \frac{1}{\sqrt{2}}S_\varepsilon & 0 & P_\varepsilon \end{pmatrix}, \tag{23}$$

where

$$P_\varepsilon=a_vC_a, \tag{24}$$

$$Q_\varepsilon=-bC_b-\left(bC_b-\frac{1}{\sqrt{3}}dC_f\right)\left(\frac{9}{4}c^4-3c^2\right),$$

$$S_\varepsilon=\sqrt{3}\left(bC_b-\frac{1}{\sqrt{3}}dC_f\right)\left(s^3c-\frac{3}{2}sc^3\right),$$

$$R_\varepsilon=\frac{\sqrt{3}}{4}\left(bC_b-\frac{1}{\sqrt{3}}dC_f\right)(3c^4-2c^2).$$

III. RESULTS AND DISCUSSION

The valence subband structure is calculated for InGaAs/InP QW's with various substrate orientations as a test example for the spin-orbit coupling effect on valence band structure. The InGaAs is lattice-matched to InP, the well width is $L_w=60$ Å, the Luttinger parameters are $\gamma_1=14.0, \gamma_2=5.4, \gamma_3=6.2$, the valence band offset $V_h=370$ meV, and the SO energy $\Delta=360$ meV are used. The

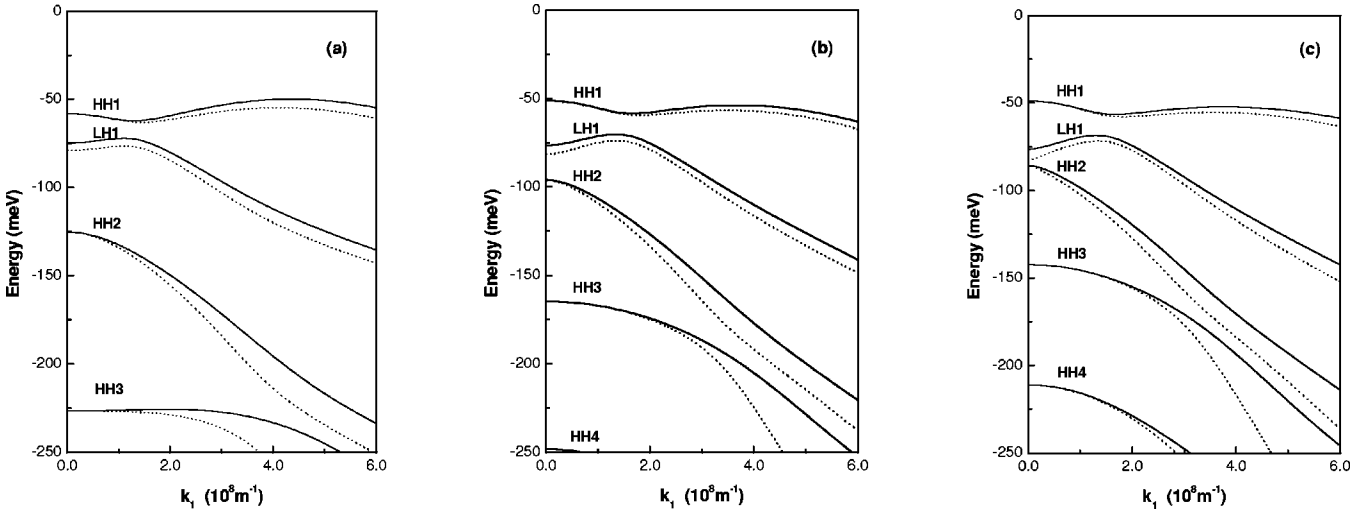

FIG. 2. Hole subbands for the quantum wells grown on (a) (11∞)-, (b) (110)-, (c) (111)-oriented substrates under the uniaxial stress $T=1.0\times10^9$ Pa.

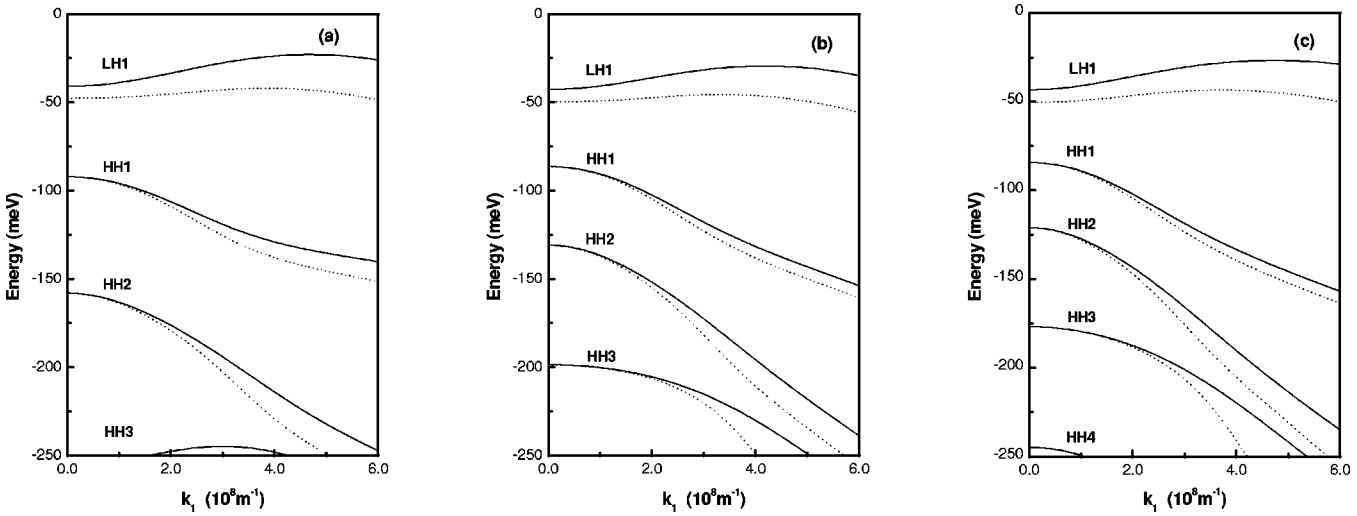

FIG. 3. Hole subbands for the quantum wells grown on (a) (11∞)-, (b) (110)-, (c) (111)-oriented substrates under the uniaxial stress $T=2.0\times10^9$ Pa.

hole subbands for the $In_{0.53}Ga_{0.47}As/InP$ QW's grown on $(11N)$-oriented substrates with $N=\infty$ [that is, (001)], 0,1 are shown in Figs. 1(a)–1(c), respectively. The solid curves are with the spin-orbit coupling and the dotted curves are without the spin-orbit coupling. At $k_1=k_2=0$, the light-hole (LH) energy levels are affected by the spin-orbit coupling in all substrate directions, which is shown by the large difference between the light-hole energies calculated with the spin-orbit coupling and without the spin-orbit coupling. In contrast, the heavy-hole (HH) energies are not affected by the spin-orbit coupling. As is shown in Eq. (13), the LH bands are strongly coupled with SO bands at $k_1=k_2=0$ in contrast to the case of HH bands which is independent from the coupling for the specific substrate orientations of (001), (111). In those cases the coupling strength between HH and SO bands is in proportion to the fractions of $(\gamma_2-\gamma_3)$, which is negligible as a reasonable approximation. However, both HH's and LH's are affected by the spin-orbit coupling at finite k_1 and k_2 so that the hole subbands are pushed upward by the SO band. The LH confinement energies are quite similar for the three substrate directions with and without spin-orbit coupling. By contrast, the HH confinement energies are reduced for (110)- and (111)-oriented substrates, reflecting the increase in effective mass. In Fig. 1(c) the position of the third heavy-hole (HH3) and LH1 is changed by the spin-orbit coupling for the (111)-oriented substrate showing that quantum confinement effects are underestimated in the model without spin-orbit coupling. This can be seen from the fact that LH1 is the fourth level in wider ($L_w=100$ Å) QW with and without spin-orbit coupling for (110)- and (111)-oriented substrates.

The hole subbands for QW's grown on $(11N)$-oriented substrates under the external uniaxial stress along the the growth direction are calculated with spin-orbit coupling. The elastic stiffness constants $C_{11}=9.991, C_{12}=4.924, C_{44}=4.887$ (10^{10} Pa) and the Pikus-Bir deformation constants $a_v=1.075$, $b=-1.753$, $d=-6.058$ (eV) are used. Figures 2(a)–2(c) and Figs. 3(a)–3(c) show the hole subbands for QW's grown on (001), (110), and (111)-oriented substrates under the uniaxial stresses $T=1.0$ and 2.0×10^9 Pa along the growth direction. The position between the second heavy-hole and the LH1 is changed at a critical stress $T=0.3\times10^9$ Pa for the (001) substrate and $T=0.4\times10^9$ Pa for the (110) and (111) cases. For (110) and (111) cases, the valence band mixing is increased by the stress below the critical stress at which the highest level changed from HH1 to LH1, resulting in an anticrossing of the HH1 and LH1 subbands. Under uniaxial stress the HH subbands are not affected by spin-orbit coupling at $k_1=k_2=0$. The LH in-plane effective mass is underestimated by ignoring the spin-orbit coupling. At a stress $T=2.0\times10^9$ Pa, the first level is LH1 and the critical stress for the HH1 and LH1 crossing over is around 1.3 and 1.4 (10^9 Pa) for (001) and (110), (111) substrates, respectively. Over the critical stress, the valence band mixing is weakened and the separation between the HH1 and LH1 is underestimated in the 4×4 model. Below the critical stress, the separation is overestimated in the 4×4 case. As quantum well width increases, the critical stress decreases because the subband splitting from quantum confinement effects decreases with the increasing well width [for example, the critical stress is around 0.7 and 0.8 (10^9 Pa) for (001) and (110), (111) substrates, respectively, in 100 Å QW].

IV. CONCLUSION

The 6×6 effective-mass Hamiltonian is derived for heterostructures grown on $(11N)$-oriented substrates. To understand the optical properties of the semiconductor heterostructures grown on the high index substrate for the device applications, knowledge of the accurate valence subband structures is required. Since the spin-orbit coupling changes the HH and the LH coupling, this gives strong effects on the anisotropy in the interband optical transitions. Therefore the inclusion of the SO band in the valence subband calculation is necessary for studying the inherent anisotropy of the high index substrates and the quantum confinement of the electronic systems. To investigate the effects of uniaxial stress in the growth direction with spin-orbit coupling, the 6×6 strain

Hamiltonian is presented. The valence band mixing is increased by the uniaxial stress below the critical value at which the HH1 and LH1 cross over. The LH1 becomes the first level and is well separated from the HH1 over the critical stress. Under high uniaxial stress, the spin-orbit coupling decreases the confinement of the LH1 due to the increased effective mass, greatly affecting the optical transition properties.

[1] Z.Y. Xu, Z.L. Yuan, B.Z. Zheng, B.S. Wang, and D.S. Jiang, R. Nötzel, and K.H. Ploog, Phys. Rev. B **51**, 7024 (1995).

[2] S.L.S. Freire, J.E.T. Reis, L.A. Cury, F.M. Matinaga, J.F. Sampaio, and F.E.G. Guimaraes, Phys. Rev. B **64**, 195325 (2001).

[3] A. Polimeni, A. Patanè, M. Henini, L. Eaves, P.C. Main, S. Sanuinetti, and M. Guzzi, J. Cryst. Growth **201**, 276 (1999).

[4] M. Henini, S. Sanguinetti, L. Brusaferri, E. Grilli, M. Guzzi, M.D. Upward, P. Moriarty, and P.H. Beton, Microelectron. J. **28**, 933 (1997).

[5] R. Nötzel and K.H. Ploog, Physica E (Amsterdam) **8**, 117 (2000).

[6] Y.F. Li, X.L. Ye, F.Q. Liu, B. Xu, D. Ding, W.H. Jiang, Z.Z. Sun, H.Y. Liu, Y.C. Zhang, and Z.G. Wang, Appl. Surf. Sci. **167**, 191 (2000).

[7] J.M. Luttinger and W. Kohn, Phys. Rev. **97**, 869 (1955).

[8] J.M. Luttinger, Phys. Rev. **102**, 1030 (1956).

[9] D.S. Citrin and Y.C. Chang, Phys. Rev. B **40**, 5507 (1989).

[10] T.B. Bahder, Phys. Rev. B **41**, 11 992 (1990).

[11] A.M. Cohen and G.E. Marques, Phys. Rev. B **41**, 10 608 (1990).

[12] A.T. Meney, B. Gonul, and E.P. O'Reilly, Phys. Rev. B **50**, 10 893 (1994).

[13] J.B. Xia, Phys. Rev. B **43**, 9856 (1991).

[14] J.J. Song, Y.S. Yoon, A. Fedotowsky, Y.B. Kim, J.N. Shulman, C.W. Tu, D. Huang, and H. Morkoc, Phys. Rev. B **34**, 8958 (1986).

[15] S. Adachi and T. Taguchi, Phys. Rev. B **44**, 10 633 (1991).

[16] C.Y.P. Chao and S.L. Chuang, Phys. Rev. B **46**, 4110 (1992).

[17] G. L. Bir and G. E. Pikus, *Symmetry and Strain-induced Effects in Semiconductors* (John Wiley & Sons, New York, 1974).